Journal of Materials Chemistry A

PAPER

View Article Online
View Journal | View Issue

Cite this: J. Mater. Chem. A, 2014, 2, 3461

High performance Pd nanocrystals supported on SnO_2-decorated graphene for aromatic nitro compound reduction†

Hongyan Li,[ab] Shiyu Gan,[ab] Dongxue Han,*[a] Weiguang Ma,[ab] Bin Cai,[ab] Wei Zhang,[ab] Qixian Zhang[a] and Li Niu[a]

Received 4th November 2013
Accepted 7th December 2013

DOI: 10.1039/c3ta14506a

www.rsc.org/MaterialsA

Promotion of the catalytic efficiency and reduction of the usage amount of Pd are crucial to developing effective and low-cost catalysts for catalytic reduction of organic aromatic nitro pollutant compound at present. Herein, we report a hybrid material of ultrafine Pd nanocrystals (PdNCs) grown on an excellent support of SnO_2-decorated graphene nanosheets (SnO_2-GNS) for a highly efficient reduction of a representative aromatic nitro compound (4-nitrophenol). The supporting material of SnO_2-GNS was prepared simply by one step of homogeneous reaction with a positively charged polymer as stabilizer and active site for absorption of the PdNCs precursor. Transmittance electronic images demonstrate that the PdNCs are densely and well covered on the SnO_2-GNS with a uniform size of 3.4 nm. This nanohybrid exhibits the fastest reduction time (4 minutes) compared to other controlled materials. Moreover, it shows high kinetic responses with an apparent kinetic rate constant (k_{app}) of 2.03×10^{-2} s^{-1} and turnover frequency (TOF) of 1.70 s^{-1}. The cycle performance (10 times) experiments demonstrate that this nanohybrid also displays a good anti-poisoning capability. Thanks to the ultrafine PdNCs, this as-prepared PdNCs/SnO_2-GNS nanohybrid may have broad potential in other catalytic fields, for example, organic synthesis, fuel cells and electrochemical biosensors.

1. Introduction

Organic aromatic nitro compounds are widely generated as by-products in different industries and agriculture,[1,2] such as colouring agents, agrochemicals and pharmaceutical products.[3] Among various aromatic nitro compounds, 4-nitrophenol (4-NP) is one of the most produced by-products,[4] which is a contaminant to the environment. In the pharmaceutical industry, 4-aminophenol (4-AP) is always derived from 4-NP by reduction. The 4-AP is well known as a vital precursor for the production of various medicines like paracetamol, phenacetin, acetanilide and antipyretic drugs *etc.*[5] It is also used widely as a photographic developer, corrosion inhibitor, anticorrosion-lubricant and hair-dyeing agent.[6] Based on this fact, it is necessary to catalyze the reduction of 4-NP into 4-AP, which can not only reduce the pollution of the environment but also make waste into treasure.

The noble metal Pd nanocrystal (NC) catalyst has attracted intensive attention due to its unique physical and chemical properties.[7,8] It has significant applications in catalysis for Suzuki coupling reactions[7,9] and in hydrogen sensors,[10] energy storage,[11–13] fuel cells[14–17] and the degradation of pollutants.[18–20] It is also worth pointing out that the reduction of 4-NP over noble metal nanocatalysts, especially Pd nanocatalysts, has been the subject of interesting investigations for the efficient production of 4-AP in the presence of $NaBH_4$.[21] For example, Morère *et al.*[22] reported a mild strategy to synthesis mesoporous silica SBA-15 as a support for Pd NCs as an advanced catalyst material for the reduction of 4-NP to 4-AP. The immobilization of Pd NCs on alumina (Al_2O_3) as a new catalyst through a simple physical precipitation method has been reported by Shailja Arora[23] for the industrial reduction of aromatic nitro compounds to amino compounds. Although these large sized Pd-based catalysts can well catalyze the reduction of 4-NP to 4-AP, their catalytic efficiency still needs to be improved in the commercial field. As it is known, the catalytic performance of the Pd nanocatalyst depends greatly on two factors: (1) the particle size; and (2) the dispersion of Pd NCs in the materials. Smaller sizes of Pd NCs will significantly enhance the surface-to-volume ratio, which leads to the further improvement of catalytic performance.[24] However, the surface energy also increases when the nanoparticle size decreases, which usually leads to serious aggregation problems.[25,26] Therefore, it remains

[a]State Key Laboratory of Electroanalytical Chemistry, c/o Engineering Laboratory for Modern Analytical Techniques, Changchun Institute of Applied Chemistry, Chinese Academy of Sciences, Changchun, 130022, Jilin, China. E-mail: dxhan@ciac.ac.cn; Fax: +86 43185262800; Tel: +86 43185262425

[b]University of Chinese Academy of Sciences, Beijing 100039, China

† Electronic supplementary information (ESI) available. See DOI: 10.1039/c3ta14506a

a major challenge to improve the stability, recyclability and catalytic activity of Pd NCs. For this purpose, it is necessary to load Pd NCs on the surface of supporting materials with low cost, high surface area, and excellent chemical and physical properties, such as metal oxides,[24,26] carbon,[27,28] polymers,[29] and so on.

In this paper, we introduced SnO_2-GNS as a new kind of building block material due to their excellent synergistic effects.[30–32] SnO_2-decorated GNS was treated with poly-(diallyldimethylammonium chloride) (PDDA), which would provide many positive charged active sites. Meanwhile, the $SnCl_2 \cdot 2H_2O$ was added into the solution to act as both the reducing agent for GNS and the precursor of SnO_2. SnO_2-GNS not only provide a platform for self-assembly of Pd NCs by electrostatic adsorption, but also prevent their aggregation. Furthermore, it was found that the as-prepared PdNCs/SnO_2-GNS nanohybrid exhibited highly efficient activity as catalyst for reduction of 4-NP to 4-AP by $NaBH_4$. In addition, other previously reported Pd-based catalysts[22,23,25,33–36] have also been compared with our PdNC/SnO_2-GNS hybrid. The results show distinctly that the as-synthesized PdNC/SnO_2-GNS exhibit a preferable catalytic efficiency. In addition, the apparent kinetic rate constant (k_{app}) and turnover frequency (TOF) of PdNC/SnO_2-GNS reach about 2.03×10^{-2} s^{-1} and 1.70 s^{-1}, respectively, which demonstrates great potential for commercial application.

2. Experimental

2.1 Chemicals

Sodium tetrachloropalladate(II) (Na_2PdCl_4 99.9%) and poly-(diallyldimethylammonium chloride) (PDDA, 20 wt% in water) were purchased from Sigma-Aldrich. *p*-Nitrophenol was obtained from Aladdin. Graphite powder (325 mesh), sodium borohydride ($NaBH_4$) and tin(II) chloride dehydrate ($SnCl_2 \cdot 2H_2O$), HCl (36–38%) were purchased from the Beijing Chemical Factory (Beijing, China). All chemicals were used as received without further purification. All aqueous solutions were prepared with ultra-pure water (>18 MΩ) from a Milli-Q Plus system (Millipore). All glassware used in the following procedures were cleaned in a bath of freshly prepared HCl : HNO_3 (3 : 1, *aqua regia*) and rinsed thoroughly with water prior to use.

2.2 Preparation of graphene oxide (GO)

Graphene oxide (GO) was prepared by oxidizing natural graphite power based on a modified Hummers method.[37] GO was then suspended in ultra-pure water to form a brown dispersion, which was further treated by dialysis for 6–7 days to completely remove metal ions and acids.[38] The concentration of the finally obtained GO product was calibrated with the UV-Vis spectra at room temperature.

2.3 Preparation of PDDA-functionalized SnO_2-GNS

SnO_2-GNS was synthesized according to previous work with minor modifications.[30,39] Briefly, 20 mL GO (0.5 mg mL^{-1}) and 0.5 mL PDDA were mixed in a round bottom flask and stirred for more than 30 minutes. Subsequently, 0.15 mL of HCl and 0.30 g of $SnCl_2 \cdot 2H_2O$ were added. The mixture was then continually stirred at 90 °C for 3 h. After the mixture was cooled to ambient temperature, it was centrifuged and washed three times with ultra-pure water. Finally, the obtained SnO_2-GNS was dispersed into 50 mL water for further use. As control, SnO_2-GNS nanocomposites were prepared under the same conditions without introduction of PDDA.

2.4 Preparation of PdNCs/SnO_2-GNS nanohybrid materials

1 mL of Na_2PdCl_4 aqueous solution (5 mM) and the as-prepared 20 mL SnO_2-GNS dispersion were mixed together while stirring for more than about 60 minutes. Then 1 mL of $NaBH_4$ (5.63 mg) was added to the above mixture. It was stored at room temperature for several hours until the $PdCl_4^{2-}$ was completely reduced. The solution was then centrifuged and washed three times with ultra-pure water. Finally, the obtained PdNCs/SnO_2-GNS nanohybrid was dispersed in 20 mL water for further experiment.

2.5 Catalytic studies

In order to investigate the catalytic activity of the as-prepared PdNCs/SnO_2-GNS, a freshly prepared 50 μL of 4-NP solution (10 mM) and 50 μL of $NaBH_4$ solution (3 M) were added to a quartz cuvette and the color of reaction system was observed to transfer from light yellow to yellow–green. Then, 3 mL of aqueous solution containing 5 μL PdNCs/SnO_2-GNS nanohybrid was injected into the cuvette, which started the reaction. The change of the intensity of the absorption peak at 400 nm of 4-NP was monitored by UV-vis spectroscopy as function of reduction time. When the solution became colorless, it indicated the accomplishment of the reaction. Afterwards, another 100 μL of mixed reagent of 4-NP (10 mM) and $NaBH_4$ (3 M) was added into the reaction system after each round of reaction. This step was repeated for nine rounds to study the stability of catalyst.

2.6 Instrumentation

Ultraviolet-visible (UV-vis) absorption spectra were recorded with a U-3900 HITACHI UV-vis spectrophotometer. Transmission electron microscopy (TEM) images were obtained on a Hitachi-600 TEM with an accelerating voltage of 100 kV. The samples for TEM images were prepared by dropping the dilute colloidal suspension (~0.05 mg mL^{-1}) onto a carbon-covered copper grid and dried in air at ambient temperature. High-resolution transmission electron microscopy (HRTEM) and energy dispersive X-ray spectroscopy (EDX) measurements were performed on a Tecnai G^2 microscope at 200 kV. X-Ray photoelectron spectroscopy (XPS) analysis was performed on an ESCALAB-MKII X-ray photoelectron spectrometer (VG Co.) with Al Kα X-ray radiation as the X-ray source for excitation. Fourier transform infrared spectra (FTIR) were collected on a Bruker Tensor 27 spectrometer. Zeta potential measurements were performed using a Zetasizer NanoZS (Malvern Instruments). Atomic force microscopy (AFM) images were obtained with Veeco Instruments Nanoscope in tapping mode. The samples

for AFM measurements were prepared by dropping the diluted colloidal suspension (~0.01 mg mL^{-1}) onto a freshly cleaved mica surface and then drying in air. The weight of the Pd in the PdNCs/SnO_2-GNS nanohybrid was determined by inductively coupled plasma (ICP) atomic emission spectrometric analysis.

3. Results and discussion

3.1 Characterization of materials

Well-dispersed GO with nanosheet structure was synthesized by the modified Hummers method in this study, which provides a raw material as the building block to self-assemble the metal nanoparticles. As shown in Scheme 1, the PdNCs/SnO_2-GNS nanohybrid was generated by *in situ* reduction of negatively charged $PdCl_4^{2-}$ precursors adsorbed on the positively charged surface of SnO_2-GNS through electrostatic attraction. Here, $SnCl_2$ not only acts as the reducing agent for GO, but also the precursor of SnO_2. Fig. 1a and b are typical TEM images of the prepared GO and SnO_2-GNS nanocomposites, respectively. It clearly shows that the as-obtained GO exhibits the appearance of a wrinkle-like thin sheet, which is a structural feature of GO nanosheets.[31] In contrast, the SnO_2-GNS nanocomposites present a well-defined nanofilm morphology.[39,40]

At the same time, in order to prove that the SnO_2 was decorated on both sides of the GNS and a uniform plane of nanoparticles was formed, further investigation by atomic force microscopy (AFM) analysis has also been performed. Fig. 1c and d are typical images of AFM of GO and SnO_2-GNS nanocomposites, respectively. They reveal that SnO_2, as the templates, were uniformly decorated on GNS. The height profile of GO is about 0.9 nm (Fig. 1e), which is similar to the original GO properties, just as reported.[41,42] The average thickness of SnO_2-GNS is found to be ~12.5 nm (Fig. 1f) due to the formation of SnO_2 and the introduction of PDDA. All of the results shown in Fig. 1 reveal that the introduction of PDDA does not change the morphology of GO.[17,43,44] PDDA plays a significant role to provide a positive charge site to attract the negatively charged $PdCl_4^{2-}$ ions *via* electrostatic interactions. Pd NCs with a small size of 3.4 nm were self-assembled directly on both sides of the SnO_2-GNS nanocomposites upon redox reaction.

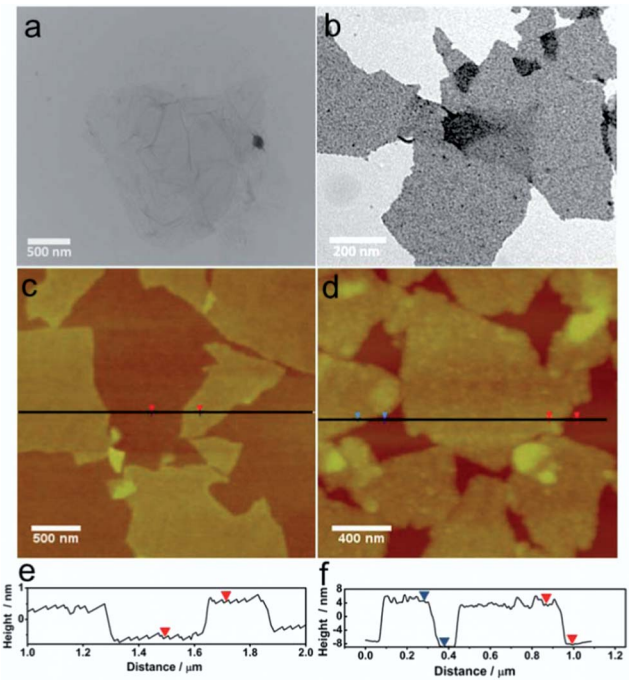

Fig. 1 TEM, AFM image of GO (a and c) and the SnO_2-decorated GNS (b and d) and their height profiles (e and f), respectively.

In order to assess the reduction of GO and formation of SnO_2-GNS, UV-vis absorption spectra (Fig. S1†) and FT-IR spectra (Fig. S2†) were recorded. The UV-vis characteristic absorption peak of GO at 230 nm disappeared and red shifted to a broad peak located at 260 nm, which indicated the reduction of GO.[40,45] In addition, the absence of the peaks at 1730 cm^{-1} (C═O) and 1421 cm^{-1} (C–OH) indicated the removal of oxygen-containing groups from GO after reduction.[45] The absorption peaks appearing at 1629 cm^{-1} (C═C) and 1460 cm^{-1} are found to be the characteristic absorption peaks of PDDA.[46]

The results of the above characterizations clearly show that SnO_2 has been successfully decorated on the surface of the GNS, which exhibit an excellent monolayer structure. Thus it provides a good platform as a new building block for self-assembly of the noble metal Pd NCs. As shown in Fig. 2a and b, the obtained PdNCs/SnO_2-GNS nanohybrids retained a well dispersed and sheet-like morphology. It was found that small nanoparticles (black dots) were self-assembled on the surface of the SnO_2-GNS and well-distributed. The high-magnification transmission electron microscopy (HRTEM) image of PdNCs/SnO_2-GNS in Fig. 2c shows a regular lattice spacing of 0.33 nm and 0.23 nm corresponding to those of the (110) plane of SnO_2 and (111) plane of Pd, respectively. Moreover, the inset of Fig. 2a shows that the as-prepared PdNCs/SnO_2-GNS have a uniform and stable state existing in the aqueous solution. At the same time, the corresponding particle size distribution histograms of the Pd nanoparticles were measured and are shown in Fig. 2d.

Furthermore, the distribution of the Pd NCs supported on SnO_2-decorated GNS could be further elucidated by

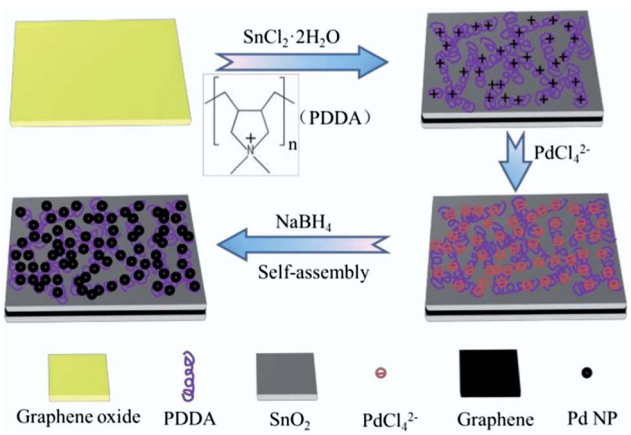

Scheme 1 Procedure to synthesise Pd NCs supported on an SnO_2-decorated graphene nanohybrid material.

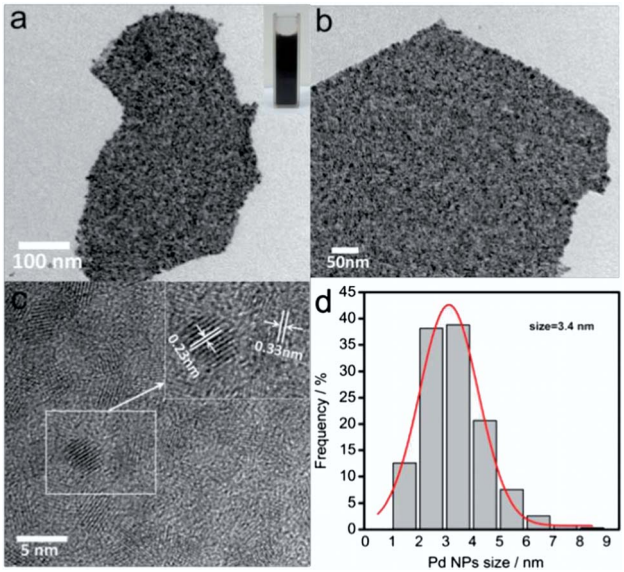

Fig. 2 TEM (a and b) and HRTEM (c) images of the PdNCs/SnO_2-GNS nanohybrid. The inset of (a) is a digital photo of the as-made PdNCs/SnO_2-GNS which has a uniform and stable state existing in the aqueous solution. (d) The corresponding particle size distribution histograms of the Pd nanoparticles.

HAADF-STEM and elemental mapping. The images of C, O, Sn and Pd of the PdNCs/SnO_2-GNS are shown in Fig. 3, which agreed well with the energy-dispersive X-ray (EDX) analysis (Fig. S3†) (the Cu element in the EDX originates from the carbon copper grid). It can be clearly seen that the Sn–L and Pd–L elements were uniformly distributed in the monolayer GNS like a "maple leaf", which suggests that PdNCs/SnO_2-GNS were well synthesized.

In order to illustrate further the composition of the PdNCs/SnO_2-GNS, X-ray photoelectron spectroscopy (XPS) was performed and is shown in Fig. 4. XPS analysis confirms the existence of C, O, N, Sn, Pd $3d_{5/2}$ and Pd $3d_{3/2}$ in the PdNCs/SnO_2-GNS, which were agreed well with the EDX and elemental mapping analysis. Compared with the C 1s XPS spectra of GO (Fig. S4a†), the PdNCs/SnO_2-GNS (Fig. 4a) display significantly decreased peak intensities of the oxygenated carbon species, which further manifest the in reduction of GO. Fig. 4b shows N

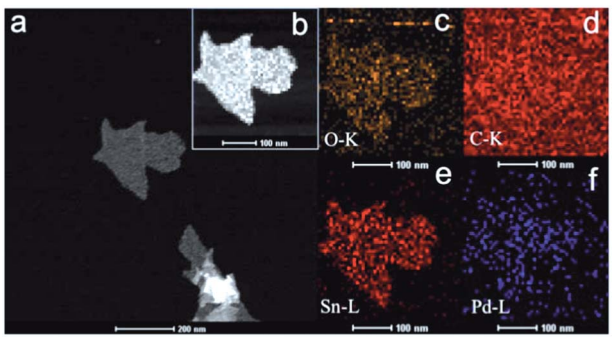

Fig. 3 HAADF-STEM (a and b) and elemental mapping images (c–f) of PdNCs/SnO_2-GNS nanohybrid.

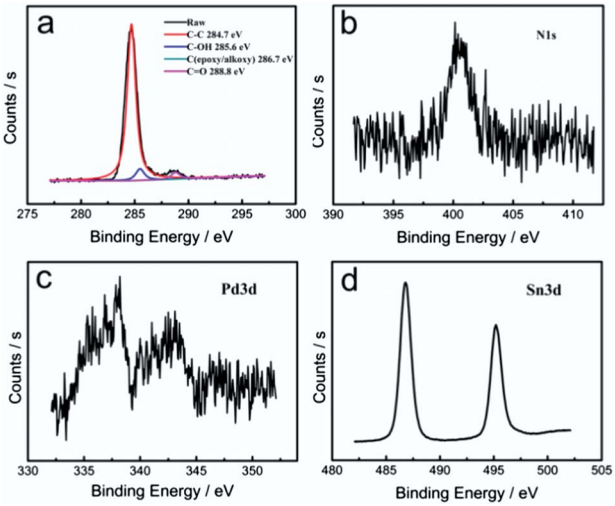

Fig. 4 (a) C 1s, (b) N 1s, (c) Pd 3d and (d) Sn 3d XPS spectra of the PdNCs/SnO_2-GNS nanohybrid.

1s which is ascribed to polyelectrolyte PDDA. The Pd 3d XPS spectrum in Fig. 4c consists of two typical peaks at around 338.2 eV and 342.7 eV, corresponding to Pd $3d_{5/2}$ and Pd $3d_{3/2}$, respectively. In the Sn 3d spectrum (Fig. 4d), two symmetrical peaks centered at 495.2 eV and 486.8 eV correspond to the Sn $3d_{5/2}$ and Sn $3d_{3/2}$ spectra, which are attributed to Sn^{4+} species. This clearly indicates the successful modification of SnO_2 on the surface of GNS. The presence of SnO_2 can be further confirmed by the O 1s XPS peak at 530.5 eV (Fig. S4b†), which corresponds to the oxygen species in the SnO_2.

It is necessary to discuss the significant role of poly(diallyldimethylammonium chloride) (PDDA) in this study. PDDA is a kind of water-soluble cationic polyelectrolyte attributed to the ammonium group and can provide a positive charge site to attract the negatively charged $PdCl_4^{2-}$ ion *via* electrostatic interaction. It also acts as a "glue" to bind the Pd NCs upon redox reaction growing *in situ* on the surface of SnO_2-GNS. The zeta potential of GO and SnO_2-GNS can also reflect distinctly the surface charge. Compared with the zeta potential of GO (−22.0 mV), that of the as-prepared SnO_2-GNS dramatically changed from a negative to positive value (+23.3 mV) after introduction to the PDDA. To a certain extent, PDDA can create a strong electrostatic repulsion "environment" surrounding the noble metal Pd NCs,[47,48] which is like a "spacer" that causes the nanosheet structure of graphene to be well dispersed in aqueous media. Another control experiment was carried out under the same conditions without introduction of PDDA, which resulted in the aggregation of SnO_2-GNS due to the absence of the electrostatic repulsion and the weak interactions in solution (Fig. S5†). From Fig. S5b,† it can also be seen clearly that the suspension of SnO_2-GNS aggregated obviously in the quartz cuvette. Therefore, it is reasonable to conclude that PDDA plays a key role in attracting the precursor of Pd NCs and their self-assembly on the surface of SnO_2-GNS, making PdNCs/SnO_2-GNS well-dispersed in aqueous media by π–π interaction and electrostatic interaction.

3.2 Evaluation of catalytic activity

The catalytic activity of the as-prepared PdNCs/SnO_2-GNS composite material was evaluated in terms of the reduction of 4-NP into 4-AP with excess $NaBH_4$ in aqueous solution. To our knowledge, this is a typical hydrogenation reaction.[21] Fig. 5a shows the time-dependent UV-vis spectra for the catalytic reduction of 4-NP by $NaBH_4$ over high performance Pd NCs supported on SnO_2-GNS. The characteristic absorption peak of 4-NP at λ_{max} = 400 nm is found to decrease gradually as a function of time, accompanied by the appearance of the freshly generated peak at 300 nm corresponding to 4-AP, which indicated the successful conversion of 4-NP to 4-AP. Simultaneously, the color of reaction system changed from light yellow to yellow–green due to the production of *p*-nitrophenolate ions after the addition of sodium borohydride. The process of catalytic reduction was monitored very quickly, within 0 to 0.5 min. In Fig. 5a, as time going on, the process gradually slowed down, until the reaction finished within 3.5 min. Based on these facts, it is found that the reduction started immediately after the addition of the catalyst and there was no induction time. Sodium borohydride is in excess during the whole process of this reaction, so the reaction can be assumed to have first-order kinetics.[29,49] In addition, the kinetic equation of this catalytic reaction could be shown as following:

$$-\mathrm{d}C_t/\mathrm{d}t = k_{app}C_t = k_{nor}c_{Pd}C_t$$

where C_t is the concentration of 4-NP at time t. c_{Pd} (mM) is the concentration of Pd presented in the system. Then, k_{app} is the apparent reaction rate constant, which can be obtained from the slope of the linear correlation. In most cases, k_{app} was normalized to the c_{Pd}, deriving k_{nor} to reveal the intrinsic catalytic activity of the catalyst.

$$k_{nor} = k_{app}/c_{Pd}$$

Fig. 5b shows C_t/C_0 *versus* the reaction time for the reduction of 4-NP over the catalyst-free, mono-SnO_2-GNS, Pd-GNS and as-prepared PdNCs/SnO_2-GNS. As is shown in Fig. 5b, the catalyst-free system and that in the presence of SnO_2-GNS display no catalytic activity. When Pd-GNS was added to the aqueous mixture of 4-NP and $NaBH_4$ alone, the reaction was found to finish in 10 minutes. However, with the addition of highly efficient Pd nanocrystals supported on SnO_2-GNS, 4-NP was rapidly reduced within 3.5 min. This means that PdNCs/SnO_2-GNS exhibits high catalytic efficiency towards the reduction of nitro aromatic compounds. Fig. 5c shows the relationship between $\ln(A_t/A_0)$ (corresponding to $\ln(C_t/C_0)$) and C_t/C_0 *versus* the reaction time t, in which A_t and A_0 correspond to the absorbance values at specific time intervals and the initial time, respectively. The curve of $\ln(C_t/C_0)$ as function of t is found to be linear with a calculated kinetic constant k_{app} 2.03 × 10^{-2} s^{-1}, which was much higher than most of the other building blocks

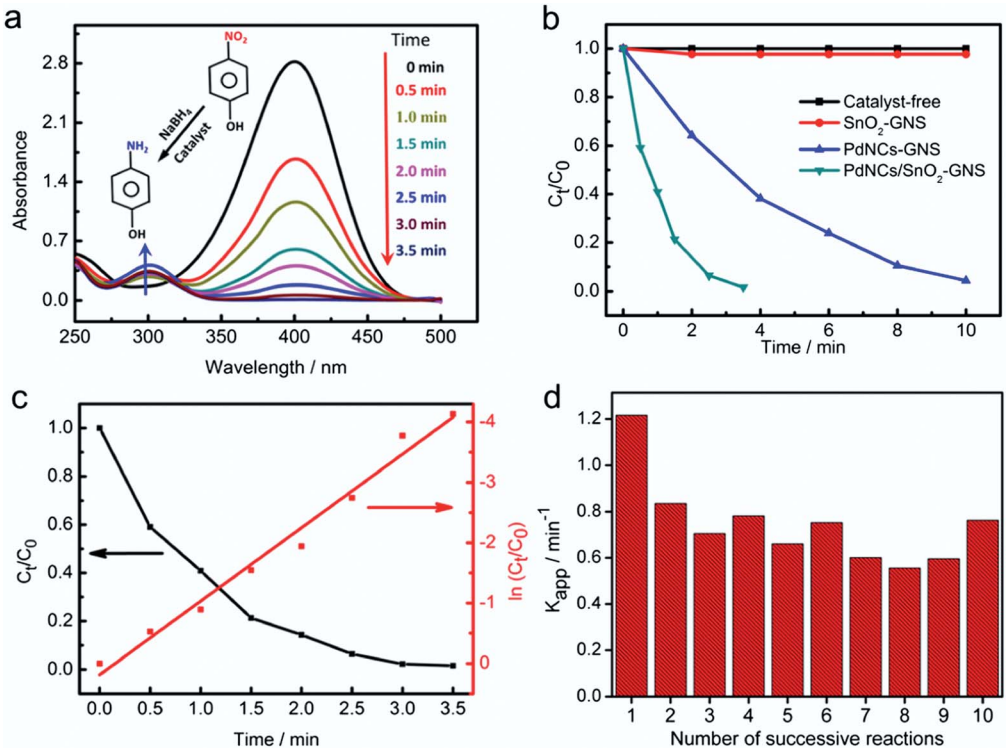

Fig. 5 (a) Time-dependent UV-vis absorption spectra for the catalytic reduction of 4-NP by $NaBH_4$ over high performance PdNCs/SnO_2-GNS (b) C_t/C_0 against reaction time for the reduction of 4-NP at different catalysts, which have catalyst-free, SnO_2-GNS, PdNCs-GNS and PdNCs/SnO_2-GNS, respectively. (c) C_t/C_0 and $\ln(C_t/C_0)$ against reaction time for the reduction of 4-NP by $NaBH_4$ over PdNCs/SnO_2-GNS. C_0 stands for the intensity of the absorption at 400 nm initially and C_t was the absorption peak at time t. (d) k_{app} against the number of successive reaction employing high performance PdNCs/SnO_2-GNS nanohybrid.

for previously reported supported Pd nanocatalysts[22,23,25,33–36] (see Table 1).

Our results are also compared with literature reports in Table 1. In order to prove further the excellent catalytic performance of the as-synthesized PdNCs/SnO_2-GNS nanohybrid, a similar size of Pd NCs was chosen as the counterparts in the control experiment. Furthermore, c_{Pd} (mM L^{-1}) was applied at the same comparison concentration of Pd presented in the system to arrive at a meaningful comparison. The content of Pd in this study is 0.02988 mg mL^{-1}, which was determined accurately by ICP atomic spectrum measurement. The turnover frequency (TOF) of the catalyst, which is defined as moles of reduced 4-NP per mole of Pd per second, is a very important parameter that is often used to compare the efficiency of catalysts. Some data of k_{nor} and TOF were not given in the literature. The as-prepared PdNCs/SnO_2-GNS showed excellent catalytic activity for the reduction of 4-NP. It has the highest k_{nor} (44.91 s^{-1} mM^{-1}) and the highest TOF (1.70 s^{-1}) among the Pd catalysts loaded on a variety of supports (Fe_3O_4/graphene,[25] SnO_2/polyaniline,[33] SBA15,[22] carbon nanotubes,[34] ZnO,[35] Al_2O_3[23] and microgel coated polystyrene (Pd/microgel-PS)[36]). It is obvious that the value of the TOF of Pd NCs loading on SnO_2-GNS (1.70 s^{-1}) is much higher than that of Fe_3O_4/graphene (1.471 s^{-1}), which indicates that the deposition of SnO_2 on GNS exhibited an excellent synergistic effect. Although the Pd NCs deposited on spherical polyelectrolyte brushes (Pd/SPB-PS) exhibit a higher k_{nor} (12.0 s^{-1} mM^{-1}), their TOF (0.228 s^{-1}) is still lower than that of the as-prepared PdNCs/SnO_2-GNS. The above results clearly show that the PdNCs/SnO_2-GNS composite hybrid obtained in our study demonstrates preferable catalytic ability compared with previously reported analogues.

It is well known that, the noble metal Pd NCs are a favorite material for many researchers due to their unique properties in the field of catalysis.[25,50] Undoubtedly, these PdNCs/SnO_2-GNS with excellent catalytic performance for the reduction of 4-NP should become a promising candidate for potential applications. However, in order to prove that the PdNCs/SnO_2-GNS also possess good potential in commercial fields, further research is needed to investigate their catalytic stability and anti-poisoning capabilities. Fig. 5d shows the values of k_{app} *versus* the number of successive reactions when employing PdNCs/SnO_2-GNS as the catalyst. As shown in the image, the catalytic activity begins to decline after the first reaction and retains almost the same catalytic activity for nine rounds of reaction. Namely, it shows an excellent stability against poisoning in the reaction system.

Insight into the mechanism of a reaction could always facilitate to overcome demerits. According to previous reports in the literature from Xia's group, we know that the poisoning of the catalyst may be caused by adsorption of the reaction product, 4-AP, on the surface of Pt NCs. In order to avoid this, the combination of Pt NCs with CeO_2 has been applied to inhibit effectively this kind of poisoning process.[26] Hence, it can be assumed that in our study the supporting material SnO_2-GNS plays a significant role which is similar to CeO_2 to avoid efficiently poisoning of the catalyst. In addition, the obtained PdNCs/SnO_2-GNS could be very easily separated through centrifugation and exhibited good recyclability.

4. Conclusion

In summary, a kind of hybrid composite material PdNCs/SnO_2-GNS has been successfully prepared *via* a simple approach, in which ultra-small Pd NCs of size 3.4 nm were distributed uniformly on SnO_2-decorated GNS. The as-prepared PdNCs/SnO_2-GNS nanohybrid exhibited excellent catalytic activity and high cycle stability against poisoning by organic aromatic compound degradation. The excellent catalytic activity should arise from the following factors: (i) the ultra-small size of the Pd NCs contributes greatly to the high performance catalytic activity; (ii) $SnCl_2$ acts not only as the reducing agent for graphene, but also as a precursor of SnO_2. It could be assumed that SnO_2 on the GNS surface acts as "linker" (anchoring sites) for Pd NCs and they are beneficial for restricting Pd NCs migration. Moreover, SnO_2 can also increase the catalytic activity of Pd NCs and demonstrates a synergistic effect between Pd NCs and SnO_2; (iii) SnO_2-GNS shows high absorption ability towards the Pd NCs precursor after the noncovalent functionalization of PDDA, which can efficiently prevent the PdNCs/SnO_2-GNS from serious aggregation; it is expected that PdNCs/SnO_2-GNS nanohybrid might be a promising candidate for potential applications such as electrocatalysis, biosensors, and energy conversion in future studies.

Table 1 Comparison of normalized rate constants (k_{nor}) and TOF of high performance Pd NCs loaded on different supports for reduction 4-NP

Samples	Pd NPs size/nm	$c_{(4\text{-NP})}$[a]/mM	c_{Pd}/mM	Pd/4-NP (mol%)	k_{app}[b]/10^{-3} s^{-1}	k_{nor}[c]/s^{-1} mM^{-1}	TOF[d]/s^{-1}	Ref.
PdNCs/SnO_2-GNS	~3.4	0.161	0.00452	0.28%	20.3	44.91	1.70	This work
Pd/Fe_3O_4/graphene	~5	1.85	0.0314	1.70%	0.061	1.943	1.471	25
Pd/SnO_2/polyaniline	~3.0	0.227	0.0166	7.31%	26.9	1.62	0.137	33
Pd/SBA15	~7	0.1	0.0629	62.89%	11.8	0.188	0.0053	22
Pd/oMWCNT	—	0.095	1.410	148%	—	—	0.07	34
Pd/ZnO	2.3	10	3.050	30.5%	—	—	0.00025	35
Pd/Al_2O_3	>5.8	0.1	0.00848	8.48%	9.2	1.085	—	23
Pd/microgel-PS	3.8 ± 0.6	0.1	0.00215	2.15%	1.5	0.698	—	36
Pd/SPB-PS	2.4 ± 0.5	0.1	0.000366	0.366%	4.41	12.0	0.228	36

[a] *c*: concentration. [b] k_{app}: apparent rate constant. [c] k_{nor}: rate constant normalized to the molar concentration of Pd. [d] Data were given or calculated in the respective papers; some data were not obtained.

Acknowledgements

The authors are most grateful to the NSFC, China (no. 21205112, no. 21225524, no. 21175130, 21105096 and no. 21127006) and the Department of Science and Techniques of Jilin Province (no. 20120308 and no. 201215091) for their financial support.

References

1 Y. C. Chang and D. H. Chen, *J. Hazard. Mater.*, 2009, **165**, 664–669.
2 S. A. Misal, D. P. Lingojwar, M. N. Lokhande, P. D. Lokhande and K. R. Gawai, *Biotechnol. Lett.*, 2013, 1–5.
3 A. Chinnappan and H. Kim, *RSC Adv.*, 2013, **3**, 3399–3406.
4 F. Wu, L.-G. Qiu, F. Ke and X. Jiang, *Inorg. Chem. Commun.*, 2013.
5 J. Li, C.-y. Liu and Y. Liu, *J. Mater. Chem.*, 2012, **22**, 8426.
6 S. Saha, A. Pal, S. Kundu, S. Basu and T. Pal, *Langmuir*, 2010, **26**, 2885–2893.
7 N. P. Cheval, A. Dikova, A. Blanc, J. M. Weibel and P. Pale, *Chem.–Eur. J.*, 2013, **19**, 8765–8768.
8 C. A. Schoenbaum, D. K. Schwartz and J. W. Medlin, *J. Catal.*, 2013, **303**, 92–99.
9 F. S. Han, *Chem. Soc. Rev.*, 2013, **42**, 5270–5298.
10 A. Ollagnier, A. Fabre, T. Thundat and E. Finot, *Sens. Actuators, B*, 2013, **186**, 258–262.
11 R. Bhandari and M. R. Knecht, *ACS Catal.*, 2011, **1**, 89–98.
12 Y. J. Lee, Y. Lee, D. Oh, T. Chen, G. Ceder and A. M. Belcher, *Nano Lett.*, 2010, **10**, 2433–2440.
13 Y. J. Lee, H. Yi, W. J. Kim, K. Kang, D. S. Yun, M. S. Strano, G. Ceder and A. M. Belcher, *Science*, 2009, **324**, 1051–1055.
14 Y. Zhao, L. Zhan, J. Tian, S. Nie and Z. Ning, *Electrochim. Acta*, 2011, **56**, 1967–1972.
15 S. Zhang, Y. Shao, H.-g. Liao, J. Liu, I. A. Aksay, G. Yin and Y. Lin, *Chem. Mater.*, 2011, **23**, 1079–1081.
16 R. N. Singh and R. Awasthi, *Catal. Sci. Technol.*, 2011, **1**, 778.
17 L. Gao, W. Yue, S. Tao and L. Fan, *Langmuir*, 2013, **29**, 957–964.
18 J. R. Chiou, B. H. Lai, K. C. Hsu and D. H. Chen, *J. Hazard. Mater.*, 2013, **248–249**, 394–400.
19 S. Bai, X. Shen, G. Zhu, A. Yuan, J. Zhang, Z. Ji and D. Qiu, *Carbon*, 2013, **60**, 157–168.
20 T. R. Mandlimath and B. Gopal, *J. Mol. Catal. A: Chem.*, 2011, **350**, 9–15.
21 N. Meir, I. Jen-La Plante, K. Flomin, E. Chockler, B. Moshofsky, M. Diab, M. Volokh and T. Mokari, *J. Mater. Chem. A*, 2013, **1**, 1763.
22 J. Morère, M. J. Tenorio, M. J. Torralvo, C. Pando, J. A. R. Renuncio and A. Cabañas, *J. Supercrit. Fluids*, 2011, **56**, 213–222.
23 S. Arora, P. Kapoor and M. L. Singla, *React. Kinet., Mech. Catal.*, 2010.
24 H. Zhang, X. Li and G. Chen, *J. Mater. Chem.*, 2009, **19**, 8223.
25 X. Li, X. Wang, S. Song, D. Liu and H. Zhang, *Chem.–Eur. J.*, 2012, **18**, 7601–7607.
26 T. Yu, J. Zeng, B. Lim and Y. Xia, *Adv. Mater.*, 2010, **22**, 5188–5192.
27 P. Zhang, C. Shao, Z. Zhang, M. Zhang, J. Mu, Z. Guo and Y. Liu, *Nanoscale*, 2011, **3**, 2943–2949.
28 Y. Fang and E. Wang, *Nanoscale*, 2013, **5**, 1843–1848.
29 S. Wunder, F. Polzer, Y. Lu, Y. Mei and M. Ballauff, *J. Phys. Chem. C*, 2010, **114**, 8814–8820.
30 C. Zhu, P. Wang, L. Wang, L. Han and S. Dong, *Nanoscale*, 2011, **3**, 4376–4382.
31 C. Zhu, Y. Fang, D. Wen and S. Dong, *J. Mater. Chem.*, 2011, **21**, 16911.
32 H. Song, L. Zhang, C. He, Y. Qu, Y. Tian and Y. Lv, *J. Mater. Chem.*, 2011, **21**, 5972.
33 X. Lu, Y. Xue, G. Nie and C. Wang, *Catal. Lett.*, 2012, **142**, 566–572.
34 H. He and C. Gao, *Molecules*, 2010, **15**, 4679–4694.
35 M.-R. Kim and S.-H. Choi, *J. Nanomater.*, 2009, **2009**, 1–7.
36 Y. Mei, Y. Lu, F. Polzer, M. Ballauff and M. Drechsler, *Chem. Mater.*, 2007, **19**, 1062–1069.
37 W. S. Hummers and R. E. Offeman, *J. Am. Chem. Soc.*, 1958, **80**, 1339.
38 D. Li, M. B. Muller, S. Gilje, R. B. Kaner and G. G. Wallace, *Nat. Nanotechnol.*, 2008, **3**, 101–105.
39 F. Li, J. Song, H. Yang, S. Gan, Q. Zhang, D. Han, A. Ivaska and L. Niu, *Nanotechnology*, 2009, **20**, 455602.
40 L.-S. Zhang, L.-Y. Jiang, H.-J. Yan, W. D. Wang, W. Wang, W.-G. Song, Y.-G. Guo and L.-J. Wan, *J. Mater. Chem.*, 2010, **20**, 5462–5467.
41 C. N. Rao, A. K. Sood, K. S. Subrahmanyam and A. Govindaraj, *Angew. Chem., Int. Ed.*, 2009, **48**, 7752–7777.
42 D. Chen, H. Feng and J. Li, *Chem. Rev.*, 2012, **112**, 6027–6053.
43 Y. Fang, S. Guo, C. Zhu, Y. Zhai and E. Wang, *Langmuir*, 2010, **26**, 11277–11282.
44 J.-D. Qiu, G.-C. Wang, R.-P. Liang, X.-H. Xia and H.-W. Yu, *J. Phys. Chem. C*, 2011, **115**, 15639–15645.
45 C. Zhu, S. Guo, Y. Fang and S. Dong, *ACS Nano*, 2010, **4**, 2429–2437.
46 K. Liu, J. Zhang, G. Yang, C. Wang and J.-J. Zhu, *Electrochem. Commun.*, 2010, **12**, 402–405.
47 H. Chen, Y. Wang and S. Dong, *Inorg. Chem.*, 2007, **46**, 10587–10593.
48 S. Zhang, Y. Shao, H. Liao, M. H. Engelhard, G. Yin and Y. Lin, *ACS Nano*, 2011, **5**, 1785–1791.
49 P. Herves, M. Perez-Lorenzo, L. M. Liz-Marzan, J. Dzubiella, Y. Lu and M. Ballauff, *Chem. Soc. Rev.*, 2012, **41**, 5577–5587.
50 M. Giovanni, H. L. Poh, A. Ambrosi, G. Zhao, Z. Sofer, F. Sanek, B. Khezri, R. D. Webster and M. Pumera, *Nanoscale*, 2012, **4**, 5002–5008.